Use of absorption optical indices to assess seasonal variability of dissolved organic matter in amazon floodplain lakes

Maria Paula da Silva[1,2]*, Lino A. Sander de Carvalho[3,4], Evlyn Novo[1], Daniel S. F. Jorge[1,5], Claudio C. F. Barbosa[3]

[1] Remote Sensing Division, National Institute for Space Research - INPE, 12227-010 São José dos Campos, Brazil
[2] Now at: Department of Analytical Chemistry, Research group BioGeoOmics, Helmholtz Centre for Environmental Research – UFZ, 04318 Leipzig, Germany
[3] Image Processing Division, National Institute for Space Research - INPE, 12227-010 São José dos Campos, Brazil;
[4] Now at: Department of Meteorology, Geoscience institute, Federal University of Rio de Janeiro, 21941-916 Rio de Janeiro, Brazil
[5] Now at: Laboratoire d'Océanologie et de Géosciences - LOG, Université du Littoral-Côte-d'Opale, CNRS, Université de Lille, 62930 Wimereux, France
Correspondence to: Maria Paula da Silva (maria-paula.da-silva@ufz.de)

Abstract. Given the importance of dissolved organic matter (DOM) in the carbon cycling of aquatic ecosystems, information on its seasonal variability is crucial. In this study we assess the use of available absorption optical indices based on in situ data to both characterize the seasonal variability of DOM in a highly complex environment and for application in large-scale studies using remote sensing data. The study area comprises four lakes located at the Mamirauá Sustainable Development Reserve (MSDR). Samples for the determination of colored dissolved organic matter (CDOM) and measurements of remote sensing reflectance (Rrs) were acquired in situ. The Rrs was used to simulate the response of the visible bands of the Multi-Spectral Instrument (MSI)/Sentinel, which was used in the proposed models. Differences between lakes were tested regarding CDOM indices. The results highlight the role of the flood pulse in the DOM dynamic at the floodplain lakes. The validation results show that the use of a_{CDOM} as a proxy of $S_{275-295}$ during rising water is worthwhile, demonstrating its potential application to Sentinel/MSI imagery data for studying DOM dynamics on large scale.

1 Introduction

Floodplain is a type of wetland characterized by a mosaic of landscapes which oscillates periodically between aquatic and terrestrial systems. This oscillation represents a key aspect in the biogeochemistry, ecology, and hydrology of floodplain lakes (Junk et al., 1989; Moreira-Turq et al., 2003). Among other effects, the flood pulse (*sensu* Junk et al., 1989) affects the proportion of autochthonous and allochthonous sources contributing to the dissolved organic matter (DOM) pool in floodplain lakes throughout the year (Melo et al., 2019).

DOM represents the largest pool of organic carbon in the aquatic environment and it has an important role in the ecosystem carbon budgets (Seekell et al., 2018; Tranvik et al., 2009; Richey et al., 2002). Besides that, DOM also controls light availability in the water column, playing a vital role in primary productivity of aquatic ecosystems and consequently fisheries

and other food webs (Hastie et al., 2019; Maia and Volpato, 2013; Volpato et al., 2004). Nonetheless, the role of DOM in the environment changes according to its quality (Inamdar et al., 2012).

DOM concentration in the environment is usually determined by the concentration of dissolved organic carbon (DOC) (Coble, 2007). However, simple measurement of DOC concentration can limit the study of the seasonal variation in the DOM quality (e.g. composition) and origin since it is related only to the bulk of DOM (Jaffé et al., 2008). Qualitative parameters are needed to better understand DOM dynamics. Ultraviolet (UV) and visible absorption measurements and fluorescence can be applied in this case as an alternative for high costly laboratory analysis (Li and Hur, 2017). Water absorption has been widely used to study DOM dynamics in streams and lakes. Based on UV and visible measurements, Helms et al., (2008) have shown that the spectral slope calculated in the range of 275 and 295 nm ($S_{275-295}$) is an indicator of DOM molecular weight and a tracer of degradation processes. $S_{275-295}$, the absorption coefficient of colored dissolved organic matter (CDOM) at 350 nm (a_{CDOM} (350)) and DOC concentration have also been used to study the dynamic of dissolved organic matter between rivers and floodplains (Spencer et al. 2008; Shen et al., 2012).

To study DOM dynamics in a wide spatial-temporal scale, satellite images have been assessed as a source of optical information about CDOM. Many studies have used Landsat images for investigating a_{CDOM} at the different wavelengths, more commonly at 350 nm, 440 nm and 420 nm (Fichot et al., 2013; Kutser et al., 2005; Zhu et al., 2014; Brezonik et al., 2015). Other study has also estimated $S_{275-295}$ from satellite data, using MODIS marine reflectance (Fichot et al., 2013). However, the reflectance of water in the visible bands may not reflect changes in the spectral slope of CDOM in the UV domain (Vantrepotte et al., 2015). Therefore, Vantrepotte et al., (2015) proposed the use of a_{CDOM} as a proxy for $S_{275-295}$ as it proved to be less affected by water optical quality and atmospheric correction. Both studies (Fichot et al., 2013; Vantrepotee et al., 2015) used MODIS data whose spatial resolution (250-1000 m) restricts the application to inland water studies. In recent years the availability of Multi-Spectral Instrument (MSI) images, on board of the Sentinel-2A (June/2015) and Sentinel-2B (March/2017), has expanded the potential of remote sensing application for DOM monitoring because of its high spatial (10 and 20 m), temporal (5 days) and radiometric (12-bit) resolutions (Toming et al., 2016). Nonetheless, it remains unclear if the use of absorption optical indices proposed in literature can be used to study DOM dynamic in a highly complex system as Amazon floodplain lakes.

The main objectives of this study are to i) investigate the variability of a_{CDOM} in floodplain lakes during the receding and rising limb of the Solimões River, ii) examine the potential of $S_{275-295}$ for distinguishing differences in DOM by comparing it in two hydrograph stage; and iii) propose an algorithm to estimate a_{CDOM} (440) as a proxy for $S_{275-295}$ using simulated MSI/Sentinel bands to support the future application of satellite remote sensing for inland DOM studies.

2 Material and methods

2.1 Study area

The study sites are four lakes located in the floodplain built at the confluence between Solimões and Japurá Rivers, near Tefé and inside the Mamirauá Sustainable Development Reserve (MSDR) (Figure 1b), a well-preserved flooded forest under low human pressure (Ayres, 1995; Castello et al., 2009; Mori et al., 2019; Queiroz, 2007). In this area, the seasonal flood is caused by both the rainfalls (in upper Amazon basin and locally - from December to May, with an average of 300 mm/month) and the annual melt of the Andean cordillera during the austral summer (Junk, 1989). Between the dry and the flood season, the variation in the water level is, on average, 12 meters at MSDR (Queiroz, 2007). The rising of the water level begins in January and goes up to late April while the water receding stage starts in July. During the flood period, which begins in May, the floodplain is occupied by water until the beginning of the receding stage (Affonso et al., 2011). The lakes were selected according to criteria defined in Jorge et al. (2017a) to guarantee access to them throughout the hydrological year and sizes compatible with the spatial resolution of the visible bands of the MSI/Sentinel 2A (10 m and 20 m). Additionally, the lakes have intrinsic differences: two of them (Buabuá and Mamirauá) are small perennial lakes surrounded by flood forest while the others (Pantaleão and Pirarara) are lakes connected to the Japurá River along the entire hydrological year, with variable size and depth in response to the flood pulse of the river.

2.2 Data source

Data were acquired in Buabuá, Mamirauá, Pantaleão, and Pirarara lakes by the Instrumentation Laboratory for Aquatic Systems team (LabISA – http://www.dpi.inpe.br/labisa) of the National Institute for Space Research (INPE-Brazil). More details about the fieldwork and measurements are provided in Jorge et al. (2017a, 2017b).

The field campaigns were carried out in March-April and July-August of 2016 which corresponds to the rising and receding water level of Solimões River, respectively. In total 87 samples were collected among the lakes and seasons.

2.3 Measurements

2.3.1 Remote sensing reflectance

The radiometric measurements to derive remote sensing reflectance (Rrs) were carried out for all sampling points, using three intercalibrated RAMSES–Trios sensors. The sensors measured above water radiance, sky radiance, and water surface irradiance, between 350 and 900 nm. During the measurements, the sensors were positioned with azimuth angles between 90° and 135° in relation to the sun and a Zenith angle of 45° to avoid sun glint effects (Mueller and Fargion, 2002). The measurement framework follows Mobley (1999). All of the measurements were made between 10:00 and 13:00 (local time) and at least 15 measurements were made at each sampling point. The dataset was processed using MSDA_XE (TRIOS, 2018) and Matlab (Mathworks, Natick, MA, USA). The Rrs estimate followed Mobley (1999), with sun glint correction based on

each sampling point. The calculated Rrs was used to simulate the reflectance of the MSI bands. For this, MSI Relative Spectral Response (RSR) of the sensor was used (Equation 1):

$$R_{rs}(B_i) = \frac{\int_{\lambda m}^{\lambda n} RSR(\lambda) \cdot R_{rs_{m(\lambda)}} d\lambda}{\int_{\lambda m}^{\lambda n} RSR(\lambda) d\lambda}, \quad (1)$$

where Rrs_m is the Rrs measured in situ and Rrs (B_i) is the Rrs simulated for the i-th band of Sentinel-2A, in the wavelength range of λm to λn. MSI RSR were taken from the user guide of the sensor (https://earth.esa.int).

2.3.2 CDOM Absorption Coefficient

Water samples were filtered first through Whatman GF/F (0.7 µm) filters (burned at 400 ºC) and then through 0.22 µm pore size polycarbonate filter. The filtrated sample was stored in sterilized dark glass bottles and kept refrigerated up to 14 days until analysis. During the analysis, all samples were kept at ambient temperature. CDOM spectral absorbance was measured with a Shimadzu UV-2600 spectrophotometer in the wavelength range between 220 and 800 nm, with increments of 1 nm and converted to $a_{CDOM}(\lambda)$ according to Equation (2) (Bricaud et al., 1981):

$$a_{cdom}(\lambda) = \frac{2{,}303 \cdot A(\lambda)}{L}, \quad (2)$$

where A (λ) is the spectral absorbance of the filtered sample in the specific wavelength λ (nm) and L is the cuvette path length (0.1 m).

The average of a_{CDOM} between 750 and 800 nm was used to correct the residual absorption spectra due to baseline drift, temperature, scattering, and refractive effects (Coble, 2007).

2.3.3 Spectral slope determination

Helms et al., (2008) have shown that the spectral slope calculated in the range of 275 and 295 nm ($S_{275\text{-}295}$) is an indicator of DOM molecular weight and a tracer of degradation processes. In the present study, $S_{275\text{-}295}$ was computed according to Equation 3 using non-linear fit (Helms et al., 2008; Bricaud et al., 1981). This function describes the $a_{CDOM}(\lambda)$ behavior along the electromagnetic spectrum and is expressed as:

$$a_{cdom}(\lambda) = a_{cdom}(\lambda_{ref}) \cdot e^{-S(\lambda - \lambda_{ref})}, \quad (3)$$

where S is the spectral slope parameter (nm^{-1}) between the wavelength interval of $\lambda - \lambda_{ref}$ and λ_{ref} is a reference wavelength (nm).

The spectral slope between the wavelengths intervals of 350-400 nm ($S_{350\text{-}400}$) was also computed in the same away describe in Equation 3. The spectral slope ratio (S_R) was calculated from the ratio between $S_{275\text{-}295}$ and $S_{350\text{-}400}$.

2.3.4 Statistical analyses

The temporal variability of DOM was assessed using a_{CDOM} (440). This wavelength was chosen due to the high CDOM absorption at low wavelengths (Jorge et al., 2017a), and is also a region used as a reference in remote sensing studies, at least, in the last thirty-six years (Bricaud et al., 1981; Brezonik et al., 2015; Bukata et al.,1995; Werdell et al., 2018).

The coefficient of variance (CV) was also computed for assessing a_{CDOM} (440) variability. Kruskal Wallis test (one-way ANOVA on ranks) with a significance level of 95% was applied to test the differences between lakes and hydrograph stages regarding a_{CDOM} (440) values as follows: i) in the first run the entire dataset was used; ii) in the second run samples from Buabuá and Mamirauá acquired during the rising period were removed.

The mean $S_{275-295}$ of the two months representing the same hydrograph stages (e.g. July and August for receding; March and April for rising) was computed for each sampling point to analyze their variability within each lake and hydrograph stage. All the statistical analyses were performed using the software Matlab (Mathworks, Natick, MA, USA).

2.3.5 Model calibration and validation

When estimating a_{CDOM} from Rrs in complex environments there is always the challenge of distinguishing the signal of CDOM and Non-Algal Particle (NAP) (Matsuoka et al., 2009; Matsuoka et al., 2012). In this study, we propose a new model for estimating a_{CDOM} (440) including the ratio between near-infrared bands to remove NAP contribution. The rationale for introducing this ratio is the null signal of CDOM and the dominance of NAP in the near-infrared range (Kirk, 2011). Previous studies also have shown that the inclusion of bands at wavelengths >600 nm increases the accuracy of the CDOM estimation model (Chen et al., 2017; Zhu et al., 2014). Thus, to determine a_{CDOM} (440), the exponential of the ratio between bands 6 (λcentral wavelength (λcw) =740 nm) and 5 (λcw = 705 nm) are subtracted from the exponential of the ratio between bands 2 (λcw = 490 nm) and 3 (λcw = 560 nm) (Equation 4):

$$a_{cdom}(440) = x \cdot e^{(B2/B3)} - (y \cdot e^{(B6/B5)} + z)\,, \quad (4)$$

where, x, y, and z are the coefficients. B2, B3, B5, and B6 are the MSI sensor simulated bands 2, 3, 5, and 6.

Monte Carlo was applied to Equation 4 to calibrate the model. Out of 42 samples collected during the rising limb, 29 were randomly selected for model calibration. This process was repeated 10^4 times and the Mean Square Error (MSE) and equation coefficients (x and y) were recorded, at each iteration.

Final model selection (most representative model based on MSE modal value) follows Augusto-Silva et al. (2014) procedure: i) construct a histogram of MSE; ii) compute mean and standard deviations of model's coefficients in the most frequent error interval; iii) rank coefficients in the range of mean ± standard deviation according to their MSE, iv) select the model with the smallest MSE.

The chosen model was validated using the 13 remaining samples (not used in the calibration process) and the final accuracy was assessed following the metrics: coefficient of determination (r^2), MSE and normalized root mean square error in percentage (%NRMSE).

3 Results

3.1 Seasonal and spatial variability of DOM

The water level of Solimões River during the sampling campaigns in the rising and receding limbs was very similar (30.04 ± 1.38 m). However, DOC concentration was almost 2-fold higher at Buabuá and Mamirauá lakes during the rising limb compared to the other samples (Table 1). During the receding limb DOC concentration was low and very similar between lakes. The same pattern was observed for the a_{CDOM} (440) (Figure 2). The highest amplitude of a_{CDOM} (440) in the entire data set (e.g. across all sites) occurred in March (1.22 to 5.46 m^{-1}) and April (1.60 to 5.97 m^{-1}) with averages of 2.56 and 3.01 m^{-1}, respectively. In July and August, the amplitude was smaller (1.32 to 2.03 m^{-1} and 1.27 to 2.19 m^{-1}, respectively) and both averaged below 2 m^{-1}. Also, higher variability (CV=52.45%) of a_{CDOM} (440) was observed at the rising limb, while in the receding limb a_{CDOM} (440) the variability (CV=14.74%) was much smaller in the lakes. The Kruskal Wallis test using samples from all lakes and dates indicated that there are significant differences ($p<0.001$) in a_{CDOM} (440) between lakes and hydrograph stages. Yet after the removal of Buabuá and Mamirauá samples acquired in March and April (rising), Kruskal Wallis results showed no significant differences in a_{CDOM} (440) values between both lakes and hydrograph stages ($p=0.51$). The two runs indicate that DOM at Buabuá and Mamirauá during the rising limb have a much higher absorption at 440 nm than those of the remaining lakes and months.

Not only differences in a_{CDOM} (440) were observed, but differences in the a_{CDOM} spectra (Figure 3). The entire set of a_{CDOM} spectra can be divided into two groups. The first group comprised Buabuá and Mamirauá spectra acquired at the rising limb, and the second group is composed of both Pantaleão and Pirarara spectra at the rising limb and the samples of all the lakes acquired during the receding limb. In the second group, it was also noticeable the presence of a shoulder between 245 and 290 nm in the absorption spectra (black arrow in Figure 3). The presence of a shoulder in the a_{CDOM} spectra can influence the calculation of $S_{275-295}$ (Xie et al., 2012), but this effect was not observed in our dataset (see supplementary material Figure S1). The mean $S_{275-295}$ of each hydrograph stage also displayed the presence of two distinct groups: one including Mamirauá and Buabuá samples, and the other, Pantaleão and Pirarara (Figure 4). $S_{275-295}$ in all samples from Buabuá and Mamirauá was near or under 0.015 nm^{-1} in the rising limb and equal or higher than 0.016 nm^{-1} in the receding limb. However, $S_{275-295}$ in all samples from Pantaleão and Pirarara was above 0.015 nm^{-1} in the rising limb and below 0.0155 nm^{-1} in the receding limb, except for one single sample from Pantaleão. Nonetheless, the average $S_{275-295}$ of each hydrograph stage was also significantly different between stages (ANOVA one-way, $p=0.03$).

The average S_R of each hydrograph stage same as $S_{275-295}$ indicated differences between the lakes surrounded by flooded forest and those near the river (see supplementary material Figure S2). The relationship between these two parameters (linear correlation, $r^2=0.9$, $p<0,001$) indicated that they can be tracking similar pools of DOM (Hansen et al., 2016).

Different values for $SUVA_{254}$ were also observed although less scatter, with values ranging from 9.44 L mgC^{-1} m^{-1} at Buabuá during the rising limb to 6.98 L mgC^{-1} m^{-1} at Pirarara during the receding limb (Table 1).

3.3 Seasonal relationship between a_{CDOM} and $S_{275-295}$

The relationship between a_{CDOM} (440) and $S_{275-295}$ varied between hydrograph stages (Figure 5). At the receding limb, $S_{275-295}$ varied between samples while a_{CDOM} (440) remained almost constant. Still, during the rising limb the variation in $S_{275-295}$ was followed by changes in a_{CDOM} (440). The relationship between $S_{275-295}$ and a_{CDOM} (440) during the rising limb is described by Equation 5:

$$S_{275-295} = 0.016\, a_{CDOM}(440)^{-0.064}, \quad (5)$$

Once the relationship between a_{CDOM} (440) and $S_{275-295}$ was established for rising water, the model for estimating a_{CDOM} (440) based on Rrs was also calibrated for this period (Equation 6):

$$a_{CDOM}(440) = 4.39^{\frac{B_2}{B_3}} + 0.59^{\frac{B_6}{B_5}} - 6.67, \quad (6)$$

Validation results showed a good explanation of the model´s variance (r^2=0.78) and predicted values close to observed values (%NRMSE=15.12, MSE=0.53 m^{-1}), indicating the feasibility of estimating a_{CDOM} (440) from Rrs (Figure 6).

4 Discussion

The water level of the rivers in the floodplain was quite similar between the sampling campaigns in rising and receding limbs, suggesting that the influence of the rivers into the lakes is similar. Thus, the flood pulse should be an important factor in the mobilization of DOM into the lakes. During the rising limb, the lakes surrounded by flood forest and close to the Solimões River have more DOM, indicated by higher DOC concentration and a_{CDOM} (440), compared to those located close to Japurá River. A large amount of DOM is also characterized by a higher degree of aromaticity (high $SUVA_{254}$) and high molecular weight (low $S_{275-295}$) at Mamirauá and Buabuá lakes, even though the chlorophyll-a concentration is higher in this lakes during this stage (Jorge et al., 2017b). The higher aromaticity and molecular weight at the rising limb is indicative of allochthonous DOM into these lakes (Melo et al., 2019; Shen et al., 2012; Spencer et al., 2008). However, at Pantaleão and Pirarara lakes, DOC concentration was low and DOM is characterized by low molecular weight during the rising limb. These distinct DOM characteristics between lakes are explained by the flood pulse of Solimões River. During the rising water level, the Solimões River inflow into the floodplain as overland flow crosses a large area of forest and carries a considerable amount of organic matter into Buabuá and Mamirauá lakes, increasing the amount of fresh-plant derived DOM. This results in more DOM of high molecular weight at these lakes. While Pantaleão and Pirarara lakes are far from Solimões River, being connected to Japurá River located in the eastern extreme of the floodplain. Therefore they are not affected by the Solimões River overland flow at the beginning of the rising limb, receiving a minor input of organic matter compared with Buabuá and Mamirauá. Therefore, at the rising limb of the hydrograph, DOM is expected to have significant differences between those lakes surrounded by flooded forests located near the Solimões River and those connected to Japurá River, located in the extreme eastern boundary of the study area (Abdo and Silva, 2004; Almeida and Melo, 2009; Carvalho et al., 2001; Henderson, 1999;

Queiroz, 2007). Yet during the receding limb this difference no longer exists and no variation in the DOM quality parameters was observed between lakes. All of them showed low DOC concentration, low a_{CDOM} (440), high $S_{275.295}$ and low $SUVA_{254.}$ As the study area consists entirely of a floodplain, during the high water the entire ecosystem is flooded. According to Ferreira-Ferreira et al. (2015), the entire area showed in Figure 1 is flooded for periods of up to 295 days in a year depending on the flood peak. A previous study in this area (Affonso et al., 2011) indicates that during the high water all water bodies become interconnected with the main channels and rivers displaying the lowest spatial variability in all limnological variables, including DOC concentration. DOC coefficient of variation among sampled water bodies dropped from 53.87% in the low water to 20.89% in the high-water of 2009 hydrological year (Affonso et al., 2011). In the Amazon basin, DOC accounts for 70% of total organic matter and floodplain areas are relevant sources of DOC to the Solimões/Amazon River (Morreira-Turq et al., 2003). Thus, due to the connection of the entire floodplain during the high water phase, it is expected that at the beginning of the receding limb the DOM quality parameters will be similar across lakes.

The shape of a_{CDOM} spectra also highlights the differences in DOM quality between the studied hydrograph stages and lakes. The presence of a shoulder in most of the spectra indicates that transformation processes are changing DOM quality. The observed feature can be a result of in situ production of protein-like materials by biological processes and/or due to photodegradation (Yamashita and Tanoue, 2009). The difference in the spectra from Buabuá and Mamirauá between the hydrograph stages can be caused by both the higher time of insolation (+35%) during receding water compared to that of the rising water (Mamirauá Sustainable Development Institute, 2018) and the entrance of fresh material during rising compared to the presence of old-degraded material during receding. Higher S_R values during receding compared to rising limb also indicate that photodegradation process are stronger during this period. Transformation processes affecting DOM quality in aquatic environments may make up for sources of DOM. Therefore, the absorption indices here analyzed demonstrate their potential to study the dynamic of DOM in the lakes.

The DOM quality dynamic between rising and receding limb was also reflected on $a_{CDOM,}$ demonstrating its importance as a monitoring parameter. Looking at large scale studies, literature reports several models relating a_{CDOM} (440) and remote sensing data, but being empirical, they are environmentally and seasonally dependent (Zhu et al. 2015). Kutser et al., (2016) tried to calibrate a model using data from Estonian lakes, Três Marias Reservoir (Brazil), and a floodplain lake located in Amazon (Curuai Lake). However, they were not able to fit a model describing the entire data set, which indicates that model development depends on DOM quality and degradation dynamics (Hansen et al., 2016). Because of the distinct dynamic of DOM observed during the hydrograph stages, in response to the flood pulse, it is rational to divide the dataset into two: rising and receding limb. At the receding limb it is difficult to draw conclusions regarding DOM origin and to evaluate DOM quality, once the DOM present in the lakes is old, highly degraded and can be originated from a mixture of different pools (Wagner et al., 2019). For the rising limb, a significant correlation between a_{CDOM} (440) and $S_{275\text{-}295}$ was found, with high (low) a_{CDOM} (440) values corresponding to low (high) $S_{275\text{-}295}$ values. The rising limb is the crucial phase in the study of DOM quality once the fresh mobilized DOM into the lakes can be differentiated from the already old and degraded DOM. Thus, DOM dynamic could be studied by remote sensing during rising limb in the floodplain lakes.

Models available in the literature to estimate a_{CDOM} usually use the ratio between green and red bands (Toming et al., 2016; Zhu et al., 2014). In this study, we tested the correlation between a_{CDOM} (440) values and the ratio between the green and red bands, but the results were poor (see supplementary material Figure S3). Thus, we proposed a new model to estimate a_{CDOM} (440), using additional bands (Equation 6). The validation of a_{CDOM} (440) model showed an accurate estimation of values, especially considering the various uncertainties related to remote sensing methods. The modelling results, therefore, are encouraging suggesting that MSI images, when available, might be applied for studying DOM properties of the Amazon floodplain lakes during the rising water level. However, the models have limitations, which are: 1) its empirical nature demanding calibration for application in other datasets; and 2) the small range of a_{CDOM} sampled (1.2 to 6.0 m^{-1}), indicating the need of new experiments including a larger number of lakes spread in a wider range of distance from the Solimões River bank, a wider span of the rising hydrograph stage and DOM molecular analyses to validate the optical indices.

5 Conclusions

The present study indicates that the use of DOM optical indices provided a deeper understanding on the connections between Solimões and Japurá Rivers flood pulse and DOM dynamics in the Amazon floodplain lakes. The results corroborates the findings in the most recent literature and indicates that there is an urgent need of research to explore new types of indices integrating both, optical spectral properties and remote sensing data. The relationship between a_{CDOM} (440) and $S_{275-295}$ stablished during one crucial hydrography stage in DOM mobilization, highlights the possibility of expanding the study of DOM dynamic by remote sensing.

The empirical model relating Rrs and a_{CDOM} (440) provided robust statistics indicating the high potential of MSI sensor for in the study of DOM. Even though this study is the first attempt of using simulated MSI data to estimate a_{CDOM} in Amazon floodplain lakes, the results herein discussed seem very promising particularly considering the new generation of satellite-borne sensors with higher temporal resolution and the resources (costs and time) involving DOM analysis in the laboratory.

Author contributions. MPdaS, LASdeC, EN and CCFB planned and designed the research. DSFJ and CCFB carried out parts of the field work and conducted a first version of data processing. MPdaS did the statistical analysis and wrote the paper with contributions from all co-authors.

Competing interests. The authors declare that they have no conflict of interest.

Acknowledgements. This study was funded by São Paulo Research Foundation (FAPESP 2014/23903-9), National Council for Scientific and Technological Development (CNPq 461469/2014-6 and CNPq 304568/2014-7) and by the project "Environmental Monitoring by Satellite in the Amazon Biome" from the Brazilian development bank (MSA-BNDES 1022114003005). Da Silva was funded by the CNPq (131242/2016-4). We are very grateful to Vitor Martins, Renato Ferreira,

Jean Farhat, Franciele Sarmento, and Dr. Waterloo Pereira Filho for their assistance during field missions. We would like to thank Dr. Helder Queiroz and the Mamirauá Institute for all the support. We also would like to thank Dr. Otávio Cristiano Montanher for the correction of flow rate data and Dr. Ivan Bergier for suggestions. We would like to thank the reviewers for their thoughtful comments and efforts towards improving our manuscript.

References

Abdo, M. S. A., Silva, C. J. Limnological characteristics of the water bodies of the Corutuba Nesting Site in Brazil's Pantanal. Acta Limnologica Brasiliensia, 6 (4), 359-368, 2004.

Affonso, A. G., Queiroz, H. L. DE, Novo, E. M. L. D. M. Limnological characterization of floodplain lakes in Mamirauá Sustainable Development Reserve, Central Amazon (Amazonas State, Brazil). Acta Limnologica Brasiliensi, 23 (1), 95–108, 2011.

Almeida, F. F., Melo, S. Limnological considerations about an Amazonian floodplain lake (Catalao lake--Amazonas State, Brazil)/Consideracoes limnologicas sobre um lago da planicie de inundacao amazonica. Acta Scientiarum, 31 (4), 387-396, 2009.

Agencia Nacional de Aguas (ANA). Hidroweb < http://www.snirh.gov.br/hidroweb/>

Augusto-Silva, P. B., Ogashawara, I., Barbosa, C. C. F., DE Carvalho, L. A. S., Jorge, D. S. F., Fornari, C. I., Stech, J. L. Analysis of MERIS reflectance algorithms for estimating chlorophyll-a concentration in a Brazilian reservoir. Remote Sensing, 6 (12), 11689–11707, doi: https://doi.org/10.3390/rs61211689, 2014.

Ayres, J. M. As matas de várzea do Mamirauá. Conselho Nacional de Desenvolvimento Científico e Tecnológico. Sociedade Civil Mamirauá, Tefé, Brasil, 99 pp, 1995.

Brezonik, P. L., Olmanson, L. G., Finlay, J. C., Bauer, M. E. Factors affecting the measurement of CDOM by remote sensing of optically complex inland waters. Remote Sensing of Environment, 157, 199–215. https://doi.org/10.1016/j.rse.2014.04.033, 2015

Bricaud, A., Morel, A., Prieur, L. Absorption by dissolved organic matter in the sea (yellow substance) in the UV and visible domains. Limnology and Oceanography, 26, 43–53. https://doi.org/10.4319/lo.1981.26.1.0043, 1981.

Bukata, R. P. J., Jerome, J. H., Kondratyev, K. Y., Pozdnyakov, D. V. Optical properties and remote sensing of inland and coastal waters. Boca Taton, Florida: CRC Press LLC, 362 p, 1995

Carvalho, P., Bini, L. M., Thomaz, S. M., Oliveira, L. G., Robertson, B., Tavechio, W. L. G., Darwisch, A. J. Comparative limnology of South American floodplain lakes and lagoons. Acta Scientiarum Maringa, 23 (2), 256-273, 2011.

Castello, L., Viana, J. P., Watkins, G., Pinedo-Vasquez, M., Luzadis, V. A. Lessons from integrating fishers of arapaima in small-scale fisheries management at the Mamirauá Reserve, Amazon. Environmental Management, 43 (2), 197–209. https://doi.org/10.1007/s00267-008-9220-5, 2009.

Chen, J., Zhu, W. N., Tian, Y. Q., Yu, Q. Estimation of colored dissolved organic matter from landsat-8 imagery for complex inland water: case study of Lake Huron. Journal of Applied Remote Sensing, 11 (3), 1–12. https://doi.org/10.1109/tgrs.2016.2638828, 2017.

Coble, P. G. Marine optical biogeochemistry: the chemistry of ocean color. Chemical Reviews, 107 (2), 402–418. https://doi.org/10.1021/cr050350+, 2007

European Space Agency (ESA). User guides <https://earth.esa.int/web/sentinel/user-guides/sentinel-2-msi/resolutions/spatial> Accessed in: June 23, 2018.

Ferreira-Ferreira, J., Silva, T.S.F., Streher, A.S. Affonso, A.G., Furtado, L. F.A., Forsberg, B. R., Valsecchi, J., Queiroz, H. L., Novo, E. M. L. M. Combining ALOS/PALSAR derived vegetation structure and inundation patterns to characterize major vegetation types in the Mamirauá Sustainable Development Reserve, Central Amazon floodplain, Brazil. Wetlands Ecol Manage (2015) 23: 41. https://doi.org/10.1007/s11273-014-9359-1, 2015.

Fichot, C. G., Kaiser, K., Hooker, S. B., Amon, R. M., Babin, M., Bélanger, S., Walker, S. A., Benner, R. Pan-Arctic distributions of continental runoff in the Arctic Ocean. Scientific reports, 3, 1053. https://doi.org/10.1038/srep01053, 2013.

Hansen, A. M., Kraus, T. E. C., Pellerin, B. A., Fleck, J. A., Downing, B. D., Bergamaschi, B. A. Optical properties of Dissolved Organic Matter (DOM): effects of biological and photolytic degradation. Limnology and oceanography, 61 (3), 1015–1032. https://doi.org/10.1002/lno.10270, 2016.

Hastie, A, Lauerwald, R, Ciais, P, Regnier, P. Aquatic carbon fluxes dampen the overall variation of net ecosystem productivity in the Amazon basin: An analysis of the interannual variability in the boundless carbon cycle. Glob Change Biol. 25, 2094–2111, 2019.

Helms, J. R., Stubbins, A., Ritchie, J. D., Minor, E. C., Kieber, D. J., Mopper, K. Absorption spectral slopes and slope ratios as indicators of molecular weight, source, and photobleaching of chromophoric dissolved organic matter. Limonology and Oceanography, 53 (3), 955–969. https://doi.org/10.4319/lo.2008.53.3.0955, 2008.

Henderson, P.A. O ambiente aquático da Reserva Mamirauá. In: QUEIROZ, H. L. & CRAMPTON, W. G. R. (Eds.). Estratégias de Manejo de recursos Pesqueiros em Mamirauá. SCM, MCT-CNPq. Brasília, Cap. 1, p. 1-9, 1999.

Jaffé, R., McKnight, D., Maie, N., Cory, R., McDowell, W. H., Campbell, J. L. Spatial and temporal variations in DOM composition in ecosystems: The importance of long-term monitoring of optical properties. Journal of Geophysical Research: Biogeosciences, 113 (G4), 2008.

Jorge, D. S. F., Barbosa, C. C., Affonso, A. G., Novo, E. M. L. DE M. Spatial-temporal characterization of optical properties of 4 lakes in the Mamirauá Sustainable Development Reserve - AM (MSDR). In: Anais XVIII Simpósio Brasileiro de Sensoriamento Remoto, Santos - SP, 2017a.

Jorge, D. S. F., Barbosa, C. C., Carvalho, L. S. DE, Affonso, A. G., Lobo, F. DE L., Novo, E. M. L. de M. SNR (signal-to-noise ratio) impact on water constituent retrieval from simulated images of optically complex amazon lakes. Remote Sensing, 9 (7), 644. https://doi.org/10.3390/rs9070644, 2017b.

Junk, W. J., Bayley, P. B., Sparks, R. E. The flood pulse concept in river-floodplain systems. In: D.P. DODGE, ed. Proceedings of the International Large River Symposium. Ottawa: Canadian Government Publishing Centre, pp. 110-127. Special Publication of the Canadian Journal of Fisheries and Aquatic Sciences, no. 106, 1989.

Kirk, J. T. O. Light and photosynthesis in aquatic ecosystems. 3.ed. Cambridge, England: Cambridge University Press, 528 p, 2011.

Kutser, T.; Pierson, D. C.; Kallio, K. Y.; Reinart, A.; Sobek, S. Mapping lake CDOM by satellite remote sensing. Remote Sensing of Environment, v. 94, n. 4, p. 535-540, 2005.

Kutser, T., Casal Pascual, G., Barbosa, C., Paavel, B., Ferreira, R., Carvalho, L., Toming, K. Mapping inland water carbon content with Landsat 8 data. International Journal of Remote Sensing, 37 (13), 2950-2961, 2016

Li, P., Hur, J. Utilization of UV-Vis spectroscopy and related data analyses for dissolved organic matter (DOM) studies: A review. Critical Reviews in Environmental Science and Technology, 47 (3), 131-154, 2017.

Maia, C. M., Volpato, G. L. Environmental light color affects the stress response of Nile tilapia. Zoology, 116 (1), 64-66, https://doi.org/10.1016/j.zool.2012.08.001, 2013.

Mamirauá Sustainable Development Institute. Database of fluviometric data from Mamirauá Sustainable Development Reserve< http://mamiraua.org.br/pt-br/pesquisa-e-monitoramento/monitoramento/fluviometrico/> Accessed in: June, 23, 2018.

Matsuoka, A.; Larouche, P.; Poulin, M.; Vinvent, W.; Hattori, H. Phytoplankton community adaptation to changing light levels in the southern Beaufort Sea, Canadian Arctic, Estuarine, Coastal and Shelf Science, 82, 537-546, 2009.

Matsuoka, A.; Bricaud, A., Bennerm R.; Para, J.; Sempéré, R.; Prieur, L.; Bélanger, S.; Babin, M. Tracing the transport of colored dissolved organic matter in water masses of the Southern Beaufort Sea: relationship with hydrographic characteristics, Biogeosciences, 9, 925–940, 2012.

Melo, M. L., Kothawala, D. N., Bertilsson, S., Amaral, J. H., Forsberg, B., Sarmento, H. Linking dissolved organic matter composition and bacterioplankton communities in an Amazon floodplain system. Limnology and Oceanography, 9999, 1–14. doi:10.1002/lno.11250, 2019.

Mobley, C. D. Estimation of the remote-sensing reflectance from above-surface measurements. Appl. Opt., 38, 7442–7455, https://doi.org/10.1364/ao.38.007442, 1999.

Moreira - Turcq, P., Seyler, P., Guyot, JL e Etcheber, H. Exportation of organic carbon from the Amazon River and its main tributaries. Hydrol. Process. 17, 1329-1344, 2003

Mori, G.B., Schietti, J., Poorter, L., Piedade, M.T.F. Trait divergence and habitat specialization in tropical floodplain forests trees. PLoS ONE, 14 (2). https://doi.org/10.1371/journal.pone.0212232, 2019.

Mueller, J.L.; Fargion, G.S. Ocean Optics Protocols for Satellite Ocean Color Sensor Validation; Revision 3; NASA TM 2002-210004; NASA Goddard Space Flight Center: Greenbelt, MD, USA, 2002; p. 308.

Queiroz, H. L. Classification of water bodies based on biotic and abiotic parameters at the várzeas of Mamirauá Reserve, Central Amazon. Uakari, 3, p. 19-34, 2007.

Richey, J. E., Melack, J. M., Aufdenkampe, A. K., Ballester, V. M., Hess, L. L. Outgassing from Amazonian rivers and wetlands as a large tropical source of atmospheric CO2. Nature, 416 (6881), 617-620. https://doi.org/10.1038/416617a, 2002.

Seekell, D. A., Lapierre, J.-F., & Cheruvelil, K. S. A geography of lake carbon cycling. Limnology and Oceanography Letters, 3(3), 49–56, 2018.

Shen, Y., Fichot, C. G., Benner, R. Floodplain influence on dissolved organic matter composition and export from the Mississippi-Atchafalaya River system to the Gulf of Mexico. Limnology and Oceanography, 57 (4), 1149-1160, 2012.

Spencer, R. G., Aiken, G. R., Wickland, K. P., Striegl, R. G., Hernes, P. J. Seasonal and spatial variability in dissolved organic matter quantity and composition from the Yukon River basin, Alaska. Global Biogeochemical Cycles, 22 (4), 2008.

Toming, K., Kutser, T., Laas, A., Sepp, M., Paavel, B., Noges, T. First experiences in mapping lake water quality parameters with Sentinel-2 MSI imagery. Remote Sensing, 8 (8), 1–14. https://doi.org/10.3390/rs8080640, 2016.

Tranvik, Lars J., Downing, John A., Cotner, James B., Loiselle, Steven A., Striegl, Robert G., Ballatore, Thomas J., Dillon, Peter, Finlay, Kerri, Fortino, Kenneth, Knoll, Lesley B., Kortelainen, Pirkko L., Kutser, Tiit, Larsen, Soren., Laurion, Isabelle, Leech, Dina M., McCallister, S. Leigh, McKnight, Diane M., Melack, John M., Overholt, Erin, Porter, Jason A., Prairie, Yves, Renwick, William H., Roland, Fabio, Sherman, Bradford S., Schindler, David W., Sobek, Sebastian, Tremblay, Alain, Vanni, Michael J., Verschoor, Antonie M., von Wachenfeldt, Eddie, Weyhenmeyer, G. A. Lakes and reservoirs as regulators of carbon cycling and climate, Limnology and Oceanography, 54, https://doi.org/10.4319/lo.2009.54.6_part_2.2298, 2009.

TRIOS. Trios sensor. 2018. Avaliable at: https://www.trios.de/en/.

Vantrepotte, V., Danhiez, F. P., Loisel, H., Ouillon, S., Mériaux, X., Cauvin, A., Dessailly, D. CDOM-DOC relationship in contrasted coastal waters: implication for doc retrieval from ocean color remote sensing observation. Optics Express, 23 (1), 33. https://doi.org/10.1364/oe.23.000033, 2015.

Volpato, G. L., Duarte, C. R. A., Luchiari, A. C. Environmental color affects Nile tilapia reproduction. Brazilian Journal of Medical and Biological Research, 37, 479-483. https://doi.org/10.1590/s0100-879x2004000400004, 2004.

Xie, H., Aubry, C., Bélanger, S., Song, G. The dynamics of absorption coefficients of CDOM and particles in the St. Lawrence estuarine system: Biogeochemical and physical implications. Marine Chemistry, 128, pp.44-56, 2012.

Yamashita, Y. and Tanoue, E. Basin scale distribution of chromophoric dissolved organic matter in the Pacific Ocean. Limnology and Oceanography, 54(2), pp.598-609, 2009

Wagner, S., Fair, J. H., Matt, S., Hosen, J. D., Raymond, P., Saiers, J., Shanley, J. B., Dittmar, T., Stubbins, A. Molecular Hysteresis: Hydrologically Driven Changes in Riverine Dissolved Organic Matter Chemistry During a Storm Event. Journal of Geophysical Research: Biogeosciences, 124 (4), 759-774, 2019.

Werdell, J., McKinna, L. I. W., Boss, E., Ackleson, S. G., Craig, S. E., Gregg, W. W., Lee, Z., Maritorena, S., Roesler, C. S., Rousseaux, C. S., Stramski, D., Sullivan, J. M., Twardowski, M. S., Tzortziou, M., Zhang, X. An overview of approaches and challenges for retrieving marine inherent optical properties from ocean color remote sensing. Progress in Oceanography, 160, 186–212. https://doi.org/10.1016/j.pocean.2018.01.001, 2018.

Zhu, W., Yu, Q., Tian, Y. Q., Becker, B. L., Zheng, T., Carrick, H. J. An assessment of remote sensing algorithms for colored dissolved organic matter in complex freshwater environments. Remote Sensing of Environment, 140, 766–778. https://doi.org/10.1016/j.rse.2013.10.015, 2014.

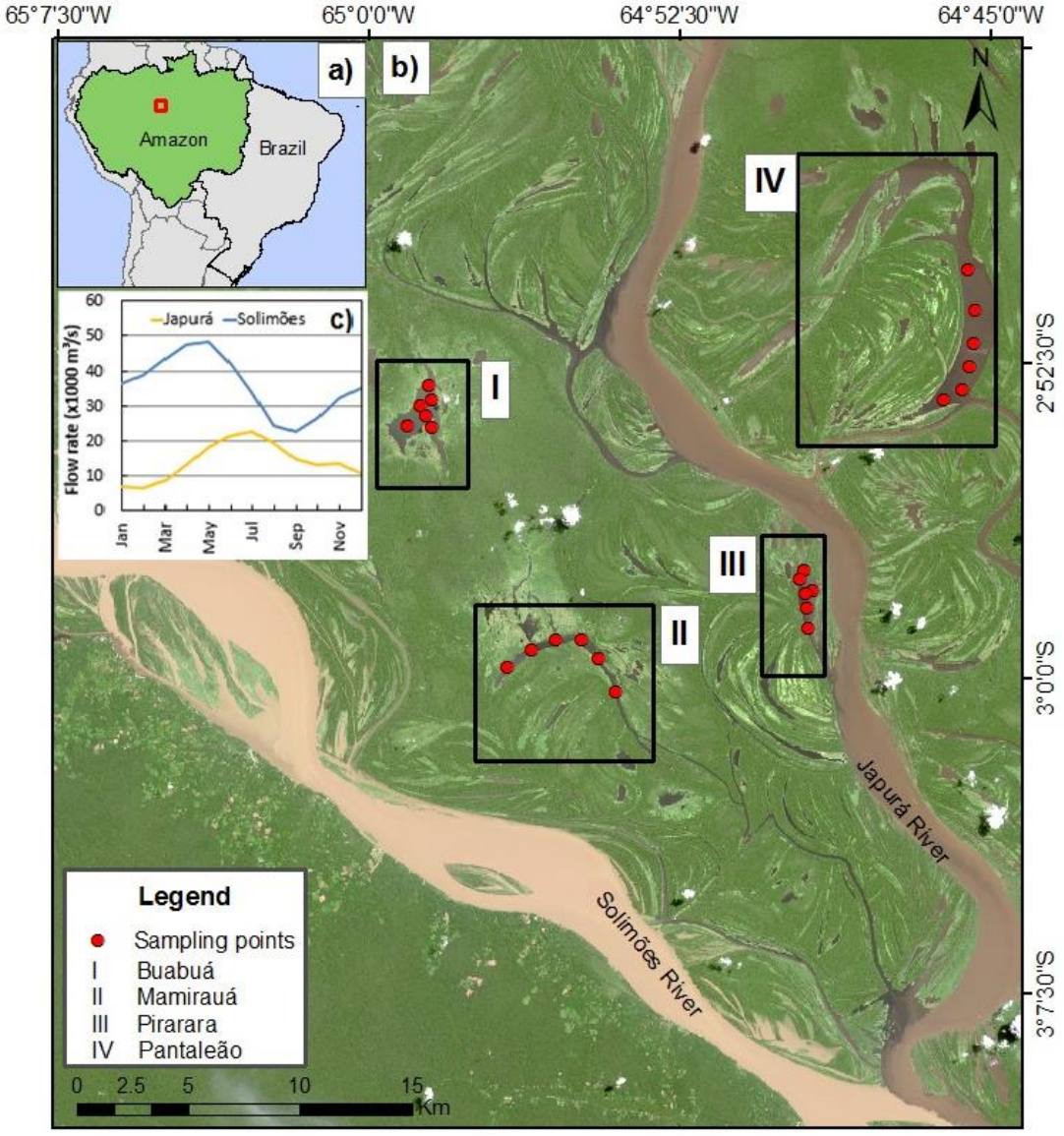

Figure 1 – Study area. (a) Overview Amazon. (b) OLI/ Landsat 8 true color image from July 30th of 2015 showing the study area and sample stations lakes: (I) Buabuá; (II) Mamirauá; (III) Pantaleão; and (IV) Pirarara. (c) Mean water flow rate (2000-2010) at Japurá and Solimões rivers calculated (Brazilian Water National Agency - ANA).

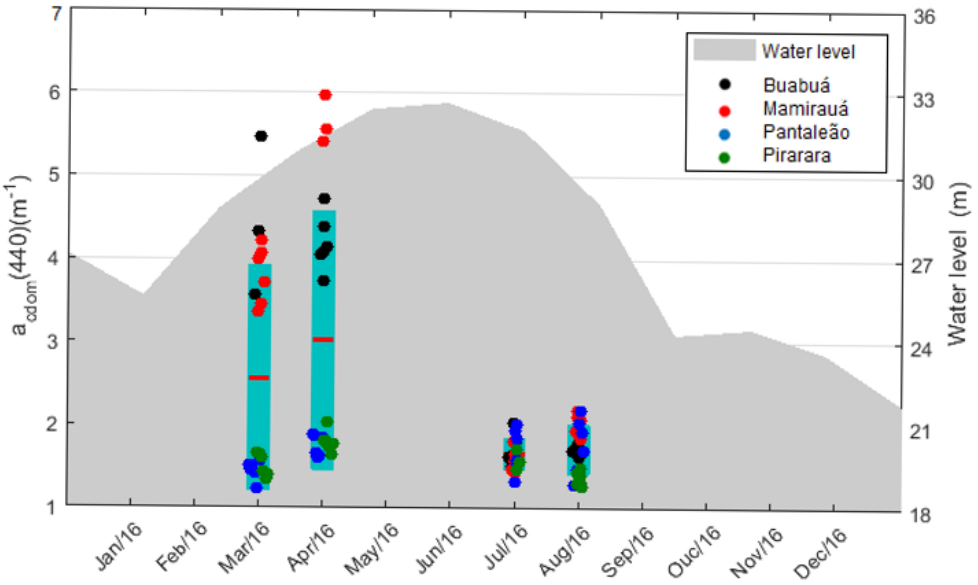

Figure 2 – Seasonal box-plot of a_{CDOM} (440) (m^{-1}) and water level (m) of Mamirauá channel in 2016. The red lines are the mean a_{CDOM} (440); each dot represent the a_{CDOM} (440) value at each sample station of lakes; and the blue boxes represent the interval between the first and third quartile. Water level was measured at Mamirauá channel (Mamirauá Sustainable Development Institute, 2018).

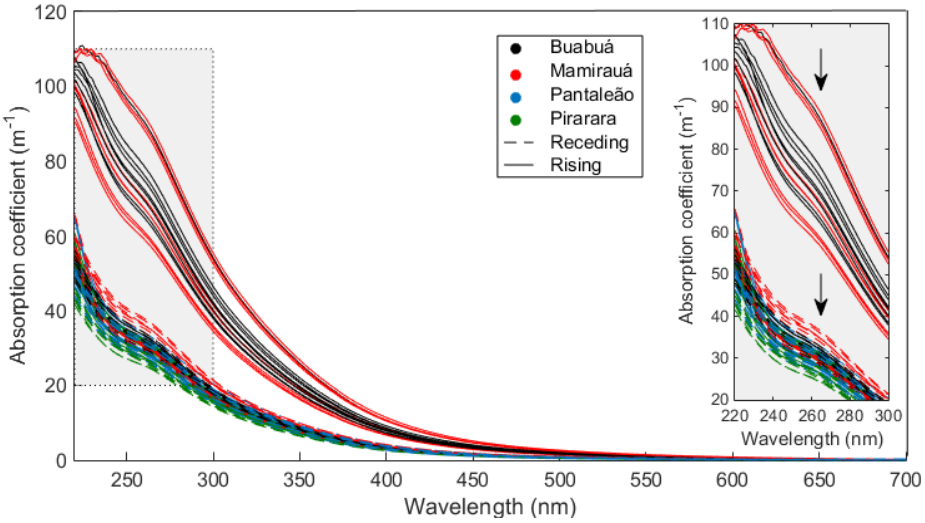

Figure 3- a_{CDOM} absorption spectra collected in Buabuá (black), Mamirauá (red), Pantaleão (blue) and Pirarara (green) lakes during rising (solid line) and receding (dash line) limb of hydrograph. The grey rectangle represents the area zoom in in the right side. The black arrows indicate the shoulder between 245 and 290 nm.

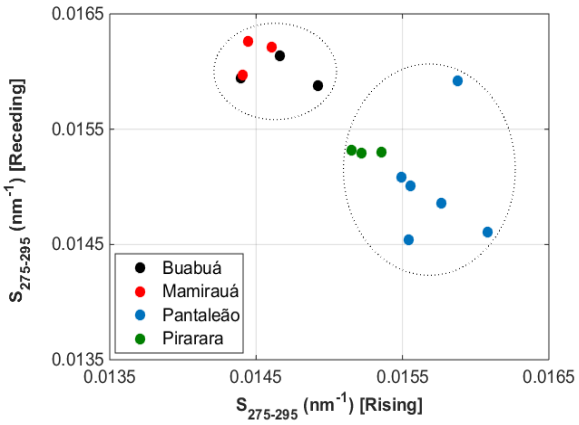

Figure 4 – Dispersion diagram of average $S_{275-295}$ (nm^{-1}) at each hydrograph stage (rising and receding) and in all lakes. The dotted ellipsis represents the two groups identified.

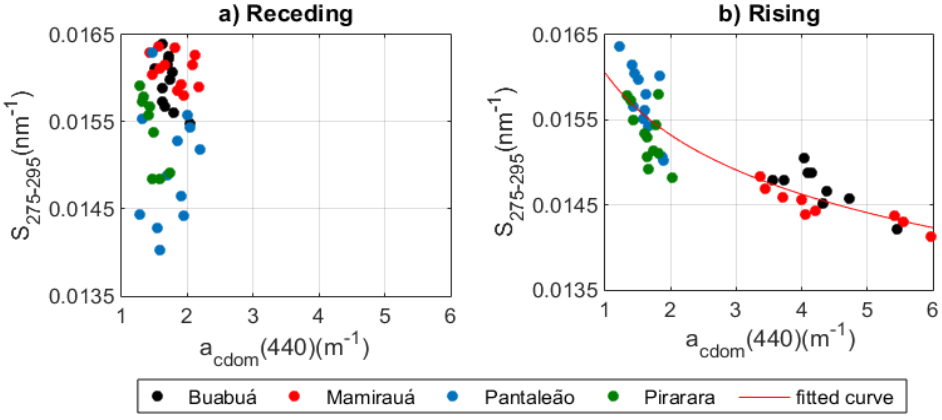

435

Figure 5 - Scatterplot of a_{CDOM} (440) (m^{-1}) versus $S_{275-295}$ (nm^{-1}) for a) receding and b) rising limb of the hydrograph.

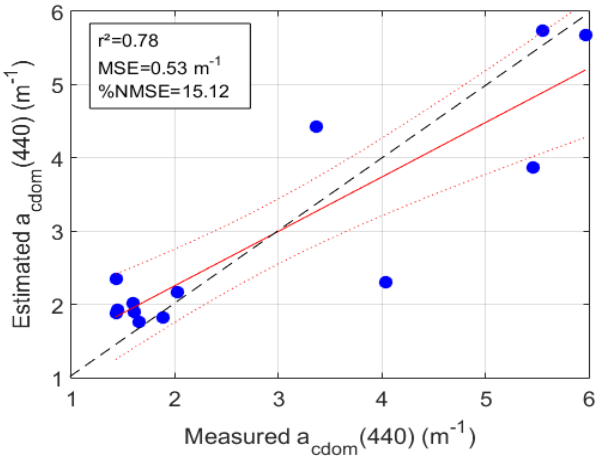

Figure 6 – Measured versus estimated a_{CDOM} (440) (m^{-1}). Equation 4 was used to estimate a_{CDOM} (440) (Y axis). The red solid line indicates the regression line between measured and estimated values; the red double dotted lines are the 95% confidence interval; and the black dashed line is the 1:1 line.

Table 1 – Overview of the sampling points.

Lake	DOC [mgL^{-1}]		a_{CDOM} (440) [m^{-1}]		$S_{275-295\ [nm^{-1}]}$		$SUVA_{254}$ [L mgC^{-1} m^{-1}]	
	Rising	Receding	Rising	Receding	Rising	Receding	Rising	Receding
Buabuá	8.20 ± 0.88	3.96 ± 0.17	4.27 ± 0.56	1.71 ± 0.13	0.0147 ± 0.0002	0.0160 ± 0.0003	9.44 ± 0.43	8.43 ± 0.52
Mamirauá	8.58 ± 1.00	4.33 ± 0.29	4.41 ± 0.97	1.80 ± 0.25	0.0145 ± 0.0002	0.0161 ± 0.0002	8.87 ± 1.09	8.22 ± 1.12
Pantaleão	5.89 ± 2.40	3.68 ± 0.35	1.59 ± 0.97	1.74 ± 0.30	0.0145 ± 0.0002	0.0150 ± 0.0000	8.32 ± 1.10	8.55 ± 1.50
Pirarara	4.15 ± 1.50	4.06 ± 0.42	1.66 ± 0.20	1.45 ± 0.14	0.0153 ± 0.0003	0.154 ± 0.0004	8.19 ± 1.73	6.98 ± 0.81

445